# Nonequilibrium Water Transport in a Nonionic Microemulsion System

Maria Minakova,[†] Alexey Savelyev,[†] and Garegin A. Papoian*,[‡]

[†]Department of Chemistry, University of North Carolina, Chapel Hill, North Carolina 27599, United States

[‡]Department of Chemistry and Biochemistry and Institute for Physical Science and Technology, University of Maryland, College Park, Maryland 20742, United States

ABSTRACT: We used microsecond time scale atomistic simulations to study the relaxation dynamics of the microemulsion water/octane/C_9E_3 system. In order to determine what transport mechanism occurs under the conditions of surfactant excess, we studied the system under a wide range of temperatures ($7-88$ °C) and showed that the surfactant acts as an effective solvent for water and carries out passive water transport through oil. Interestingly, most of surfactant-solubilized water is situated between surfactant and oil layers and is not homogeneously distributed in the surfactant—oil slab. With raising the temperature, the larger aggregates are allowed to travel through the oil layer, increasing overall water presence in oil. Also, our cluster analysis indicates that most complexes do not form a dense water core, supporting the "hydrated surfactants" transport mechanism.
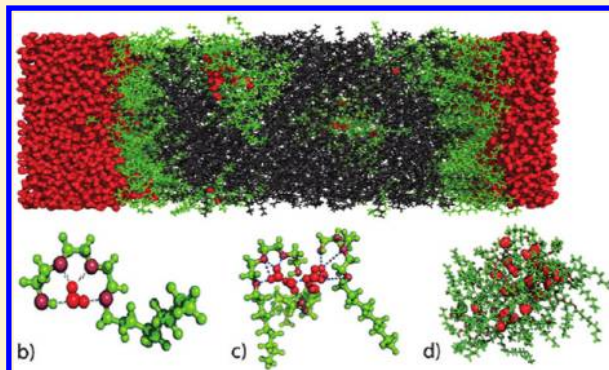
INTRODUCTION

Microemulsions have been of great fundamental and industrial interest for many decades.[1] In addition to the rich morphological behavior, microemulsions have a valuable property to store and transport small and macromolecules, allowing a wide range of applications, including drug storage and release, oil recovery, textile cleaning, preparation of various cosmetic products and perfumes, and the food industry.[1]

Water transport as a particular example of mass transport has great importance in membrane and microemulsion science, especially for biological systems. Although water transfer has been more extensively studied in application to synthetic and biological membranes,[2-11] passive (diffusive) and active (usually osmotic) water transport in various emulsions and microemulsions have also been investigated.[4,12-20] On the macroscopic scale, in the absence of osmotic pressure, coalescence is believed to be a major transport mechanism.[21] On the mesoscopic scale, it was suggested that water transport could occur through the formation of reverse micelles,[4,14] spontaneous emulsification,[16,17] hydrated surfactants,[12] and diffusion of single molecules.[18] All of these mechanisms have been observed under different conditions, but no unified picture has been created so far. Consequently, most of the available knowledge on molecular transport in microemulsions was obtained mainly from the macroscopic scale measurements, which do not provide direct atomistic insight.[4,12,17,22]

To shed light on the microscopic mechanisms of water transport, molecular dynamics (MD) simulations with all-atom (AA) resolution can be used. Although it is challenging to study long timescale phenomena with AA MD simulations, they give more detailed and thorough view of the dynamical behavior of a system. In particular, they do not contain strong simplifications that are characteristic of coarse-grained computational models. In this work, we used atomistic replica exchange molecular dynamics (REMD) simulations to investigate a nonionic ternary mixture of water/octane/C_9E_3 [nonyl tri(ethylene oxide)] at various temperatures, with an oil thickness of the nanoscale size.

The main goal of our work was to examine how water permeation occurs in a system with surfactant-rich phases. Since there is a high energetic cost to increase the area per amphiphilic molecule at equilibrium, complex formation and transport cannot be observed in equilibrated systems on the time scales available for the MD simulations, unless there is a biased force acting perpendicular to the leaflets[23-27] or a concentration gradient of a solute (ions, surfactant molecules, and etc.) in the system.[27,28] In particular, the compression or saturation of surfactant leaflets is a useful technique, allowing one to create a difference of the surfactant chemical potential inside and outside of the leaflet and to initiate active transport.[29-31]

We chose the approach similar to the latter due to its implementational simplicity and conceptual correspondence to many experimental setups. The difference in composition creates a difference in chemical potentials of the dispersed molecules, which in turns generates osmotic pressure and a compound flux. The necessary time to achieve an equilibrium state can be quite long; however, this simulation setup allows studying microscopic details about transport phenomena and relaxation dynamics in the initial response of the system.

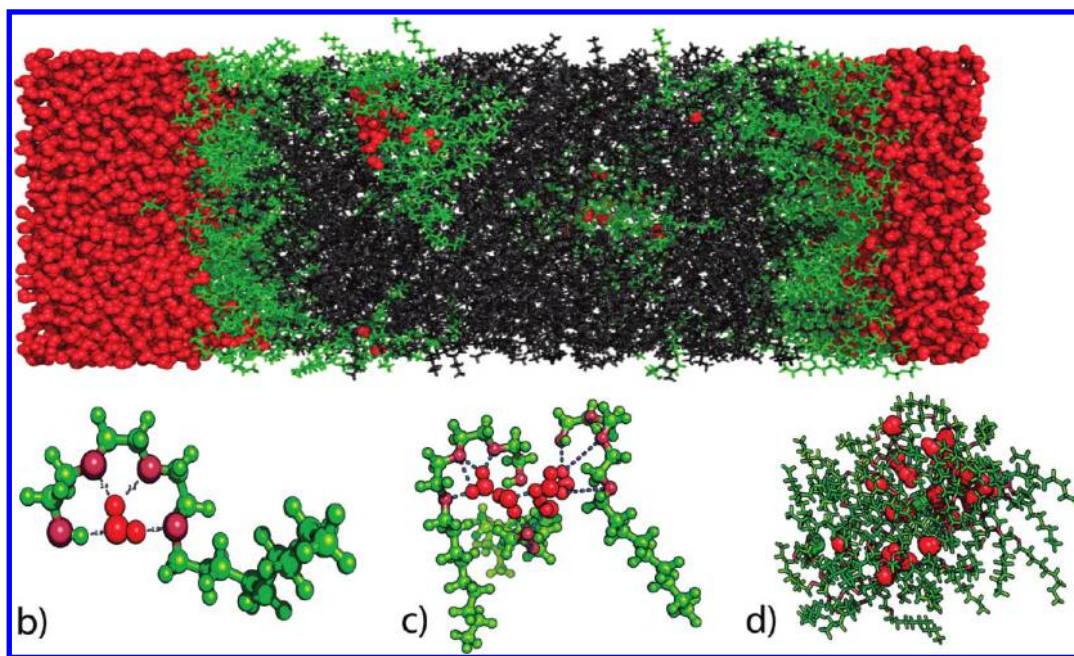**Figure 1.** (a) A snapshot of the system in a box at $T_1 = 25$ °C. Color scheme: water molecules are red, surfactant molecules are green, and oil molecules are gray. The water–surfactant complexes formed at the boundary of/in the oil layer can be seen. (b) A snapshot of a single surfactant molecule solvating one water molecule. Color scheme: green spheres are surfactant carbons and hydrogens, ruby spheres are surfactant oxygens, and red spheres are water hydrogens and oxygens. (c) A snapshot of several surfactant molecules solvating several water molecules. The color scheme is the same as that in (b). (d) A snapshot of a micellar-like aggregate, including surfactant molecules (green) and water (red). Oil molecules in (b–d) are removed for the lucid demonstration of the water–surfactant complexes.

One of our particular goals was to investigate the way surfactants mediate such water transport, because it could go through independent diffusion, inverse micelles, hydrated surfactants, or even channel formation processes. We also studied water–surfactant complexes' statistics (clustering combined with number fraction distributions) and chemical interactions (visual analysis combined with radial distribution functions). We highlight our findings in the context of prior models of water transport.

■ METHODS SECTION

MD Simulation Protocol. We have built an atomistic ternary system of water/octane/C_9E_3 [nonyl tri(ethylene oxide)], with constituents placed in a desired geometry of 5 alternating layers, water/surfactant/octane/surfactant/water (see Figure 1). The AMBER10[32] suit of programs was used for system initialization and all-atom MD simulations. First, we prepared octane and surfactant molecules because they do not enter the standard molecular database of the AMBER10 package. To generate topology files and also to assign the general AMBER force field (GAFF) parameters[33] for these molecules, we used the Antechamber module[34] of the AMBER10 package. Water molecules were parametrized according to the TIP3P model.[35] The initial structure of a five-layer system, with octane and surfactant molecules being perfectly aligned along the z-direction, was built using the Biochemical algorithm library (BALL).[36] The composition of the ternary mixture has been chosen to be $\%_{weight}$ water ≈ 0.301, $\%_{weight}$ surfactant ≈ 0.327, and $\%_{weight}$ oil ≈ 0.372. Specifically, the system was comprised of 5776 water molecules, 338 surfactant molecules, and 1125 oil molecules. The average area per surfactant molecule is $\sim$21.3 Å^2, which is smaller than

the equilibrium range of 40–50 Å^2 for similar surfactants. This setup allows us to observe fast response of the system, once the relaxation dynamics is started. The total number of atoms is 63,816, and the system is placed in a rectangular box having dimensions of $60 \times 60 \times 160$ Å^3. This is the largest all-atomistic ternary microemulsion system simulated to date.[37−39]

The initial conformation was first equilibrated at $T = 500$ K in the NPT ensemble in order to melt the oil layers and the surfactant tails, followed by the graduate temperature decrease to 300 K and subsequent switch to the NVT ensemble with a total equilibration time of $\sim$30 ns . Periodic boundary conditions were imposed in all directions. The productive run was performed by replica exchange molecular dynamics (REMD) for 42 replicas of the system in the temperature range of 280−361 K (7−88 °C). The temperature difference between neighboring replicas was 1.93 °C, which set an average probability of an exchange to 0.33.[40] A time range between switches was chosen to be 0.8 ps.[41] The total simulation time was $\sim$26 ns for each replica, which summed up to 1 μs for all replicas. Because of the large system size, the UNC Topsail supercomputer was used to perform simulations in the parallel regime with the four nodes usage per replica.

Cluster Analysis. To characterize water and surfactant association into the complexes of varying sizes, we implemented two clustering algorithms based on a reiterative sorting procedure applied to water and surfactant molecules participating in hydrogen bonds. The first one-dimensional (1D) clustering approach considered "water–water" connectivity only. Two water molecules were considered to form a link (hydrogen bond) if the distance between the oxygen (any hydrogen) of the first molecule and any hydrogen (the oxygen) of the second molecule was less or equal to a certain threshold value $l_{cl,ww}$.

The second approach is technically similar yet has a different topological concept. It accounts not only for the water—water contacts but also for the water—surfactant and surfactant—surfactant contacts, taking into account intermolecular connectivity in the clusters. In such a way, if the distance between any two heavy atoms (oxygen or carbon) of water and surfactant or surfactant and surfactant molecules was less than $l_{cl,ws}$, the corresponding molecules were considered to be associated with each other.

The numerical values of these thresholds were set to the size of the first solvation shell for each pair of molecules ($l_{cl,ww} = 3.1$ Å, $l_{cl,ws} = 3.8$ Å). The latter was determined, in turn, from the corresponding water—water, water—surfactant, and surfactant—surfactant atomistic radial distribution functions (RDF).

After that, lists of links between water and surfactant molecules were used in the recursive iterations, which are briefly described below. At the first sorting, one arbitrary molecule is put to the first cluster; then, all molecules linked with the chosen one (neighbors) are also added into the first cluster. At the second and the subsequent sorting cycles, all neighbors of neighbors are added into the cluster. Sorting is preformed until the cluster size stops increasing. Then, one of the molecules not added to the first cluster is included in the second cluster, and the procedure is subsequently repeated until all water and surfactant molecules have been sorted.

As a result, the cluster size probability distribution function $P(M,N)$ was obtained by histogramming clusters with respect to their sizes (M is the number of water molecules, and N is the number of surfactant molecules involved) and averaging this distribution over all simulation snapshots for the corresponding temperature.

We also checked how the cluster size $P(M,N)$ depends on the value of the link parameter $l_{cl,ww}$ because it was particularly important due to the relation to the "inverse micelle" water-transport mechanism. Namely, if the marginal distribution of water cluster sizes $P'(M) = \sum_N P(M,N)$ showed a maximum at the $M > 1$, it would indicate that the dense water core formation commonly occurs. This, in turn, would provide strong support for the inverse micelle water-transport model.

Clustering analysis was, therefore, performed for the following set of l_{cl}: 2.5, 2.7, 3, 3.5, 4, 5, 6, and 7 Å, at 25 °C. All resulting cluster size probability distributions $P'(M)$ have a maximum value around unity, although, for 7 Å, $P'(M)$ showed low broad peaks (probability value less than 0.1) for some values $M > 5$. With a growing value of $l_{cl,ww}$, $P'(M)$ becomes wider but preserves its shape.

In addition to that, we calculated the average ratio $\langle M/N \rangle$, which shows how many surfactant molecules per water molecule are in a cluster. We compared $\langle M/N \rangle$ for all temperatures and found that $\langle M/N \rangle$ is conserved within the 2—3 range. At the same time, the maximum of $P(M,N)$ (most probable value) was found for $\langle M/N \rangle$ within the 1—2 range for any M and all temperatures.

■ RESULTS AND DISCUSSION

The preparation of the initial configuration was performed in a such way that there would be an excess of surfactant molecules in the leaflets, thus providing no energetic penalty for the surfactants to leave the layers of residence. At such circumstances, it would be straightforward to expect active surfactant permeation of the oil layer, which might cause passive water transport as well.
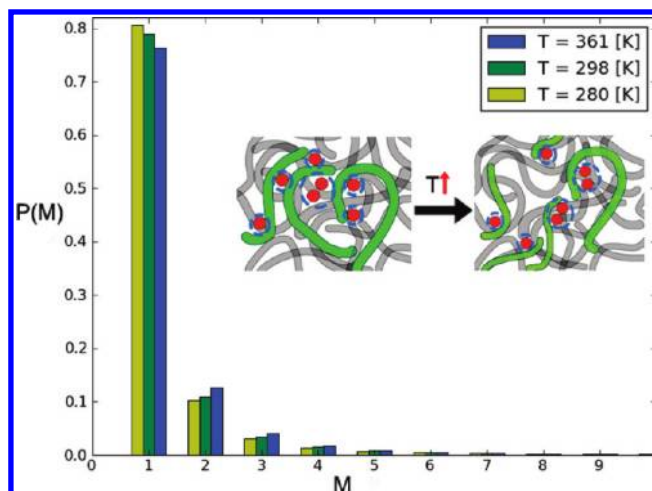

Figure 2. Probability distribution function $P(M)$ for 1D clustering of water molecules shown for several temperatures T = 7, 25, and 88 °C. The most probable cluster size is given by the maximum of $P(M)$ and is equal to 1 for all temperatures. With the temperature increase, the probability distribution becomes wider, suggesting that larger clusters are permitted in the hydrophobic region. This effect is partially due to the overall increase of the water density on the oil slab. The change in the clusters' distribution with temperature provided by the visual analysis is schematically shown in the inset. Color scheme: water molecules are red, surfactant molecules are green, and oil molecules are gray. Note the difference between the clusters obtained from 1D and 2D clustering (see Figure 3).

It should be noted that at the equilibrium surfactant density in the leaflets, one cannot observe the formation of water—surfactant complexes at the submicrosecond time scales. To verify that, we constructed a microemulsion system containing a very similar $C_{10}E_4$ surfactant, water, and octane with the same volume fractions but the equilibrium value of the area per surfactant of $A_0 \approx 44$ Å^2. Neither significant water permeation into the oil layer nor the water—surfactant complex formation were observed in this system for a wide range of temperatures during the ~2μs of the REMD simulations. Therefore, we suggest that the formation of such aggregates at the time scales smaller than 1 μs is provided by the nonequilibrium effects in the microemulsion system containing C_9E_3 surfactant. Accordingly, the focus of the current paper is on the C_9E_3 microemulsion system, and the extensive analysis of the equilibrium $C_{10}E_4$ microemulsion system will be presented elsewhere.

A typical MD simulation snapshot along with various water—surfactant complexes is shown in Figure 1. The central observation of the present study is the formation of the water—surfactant complexes in the surfactant/oil layer as a result of relaxation dynamics of the surfactant-rich leaflets, which primarily contain surfactant molecules along with oil molecules penetrating from the oil slab and water molecules dragged in by the surfactant molecules. We observed such aggregates at all stages of the MD simulation. Additionally, visual inspection suggested that water—surfactant complexes actively permeate surfactant and oil layers of the ternary mixture and vary in sizes.

Therefore, for a more quantitative description of the water permeation process, we implemented two clustering algorithms. The first approach was based on statistical histogramming of all water clusters in the system with respect to their sizes. Two water molecules were treated as belonging to one cluster if the
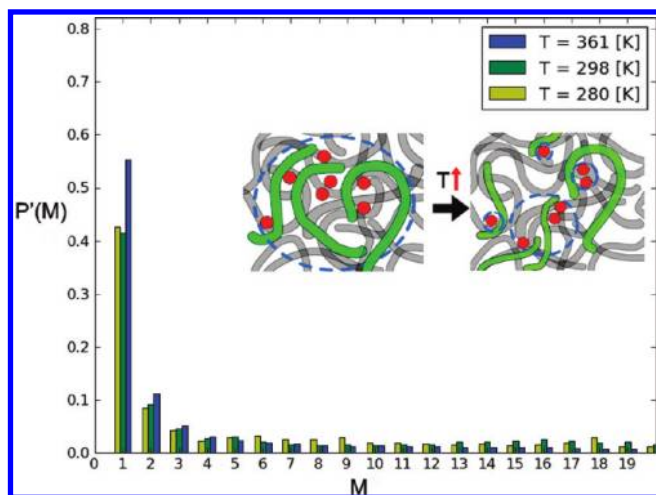
6505

dx.doi.org/10.1021/jp201431u |J. Phys. Chem. B 2011, 115, 6503–6508

Figure 3. Marginal probability distribution function $P'(M)$ for 2D clustering of water molecules shown for several temperatures $T = 7$, 25, and 88 °C. The most probable cluster size is given by the maximum of $P'(M)$ and is equal to 1 for all temperatures. With the temperature increase, the probability distribution becomes narrower, suggesting that clusters dissociate into smaller ones in the hydrophobic region. The change in the clusters' distribution with temperature provided by the visual analysis is schematically shown in the inset. Color scheme: water molecules are red, surfactant molecules are green, and oil molecules are gray. Note the difference between the clusters obtained from 1D and 2D clustering (see Figure 2).

Figure 4. RDF of various atom pairs of water and surfactant that can potentially contribute to hydrogen bond formation in the oil slab. Because our main interest is the water—surfactant complexes in oil, these RDFs has been computed for the molecules located in the oil layer. The notations for RDF atom pairs are shown in the inset, which is a snapshot of a water—surfactant complex taken from the simulations.

oxygen—hydrogen distance was less than the size of the first solvation shell, taken from corresponding radial distribution functions (see Figure 4). After the clustering procedure, they were histogrammed by a number of water molecules in a cluster, thus providing a probability distribution function $P(M)$ at a particular temperature (see Figure 2). It is important to mention that such a 1D water clustering algorithm accounts only for the water complexes that are directly connected through hydrogen bonding and does not take into account the role of surfactant molecules in these processes. As shown in Figure 2, the most probable size of water clusters is 1, which means that the number of larger clusters is insufficient and water penetration happens mostly without dense water core formation. This observation needed further investigation to elucidate whether a single water molecule diffusion or the surfactant-mediated permeation was the most probable transport mechanism.

For this reason, the second clustering algorithm has been implemented to obtain the 2D cluster size probability distribution $P(M,N)$, where P is a probability to find a cluster with M waters and N surfactants. We found that $P(M,N)$ reaches a maximum for the N/M ratio in the range of $\sim 1-2$ for all M. Yet, the average number of surfactants per water molecule in a cluster is $\langle N/M \rangle \approx 2-3$, indicating that water sharing of a surfactant polar cage commonly occurs in the complexes. Nevertheless, the marginal distribution of water cluster sizes $P'(M) = \sum_n P(M,N)$ peaks around unity, as shown in Figure 3; hence, most of the water molecules in the oil layer prefer to aggregate with surfactant molecules (hydrated surfactants) instead of forming water clusters (dense core), surrounded by a shell of surfactant molecules, where the latter structure would correspond to inverse micelles.

To further characterize the formation of the water—surfactant complexes, we tested whether any specific chemical interactions
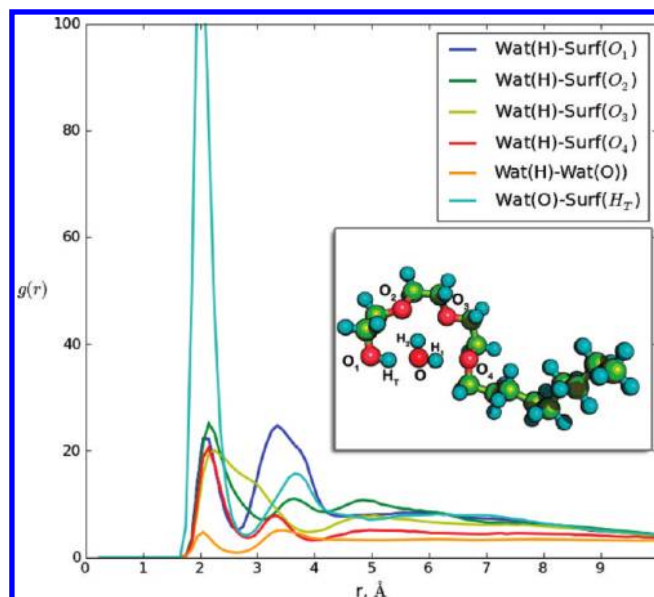
are responsible for the solvation of water by surfactant molecules. We calculated a set of RDFs among various atoms of the water and surfactant molecules (e.g., water oxygens and surfactant head's terminal hydrogens). Because there can be a significant number of possible hydrogen—oxygen atom pairs in this system, we show only RDFs with the most pronounced first and second solvation peaks (see Figure 4).

The comparison among various RDFs revealed an interesting structural property of water—surfactant complexes, namely, the hydrogen bond formation between the water oxygen and the terminal surfactant hydrogen is much more common than any other possible hydrogen bonding in the oil—surfactant layer. This is confirmed by the significantly higher first solvation peak of the water oxygen—surfactant terminal hydrogen RDF compared to that of all possible water hydrogen—surfactant oxygen RDFs in the surfactant—oil layer. This point is illustrated in the Figure 4 inset as well, where a typical water—surfactant complex is shown.

A discussion above suggests that the main stabilizing mechanism for the water solvation by surfactants is hydrogen bond formation among water oxygens and the terminal hydrogens of the surfactant head groups. It is important that the water solvation cage is highly dynamic, so that a single water molecule can be solvated by multiple surfactants or move from one polar cage to another within an aggregate, as well as share one solvation cage with other water molecules (see Figure 1c and d).

Visual analysis of the MD simulation movie revealed another compelling observation, that large water—surfactant complexes are found at the surfactant—oil interface and do not travel through the oil layer unless the temperature is very high (70—80 °C). There was seemingly a two-step process of the water transportation in the microemulsion system, where, at first, water molecules were accumulated in water pockets located within the surfactant layers and, then, one to several water
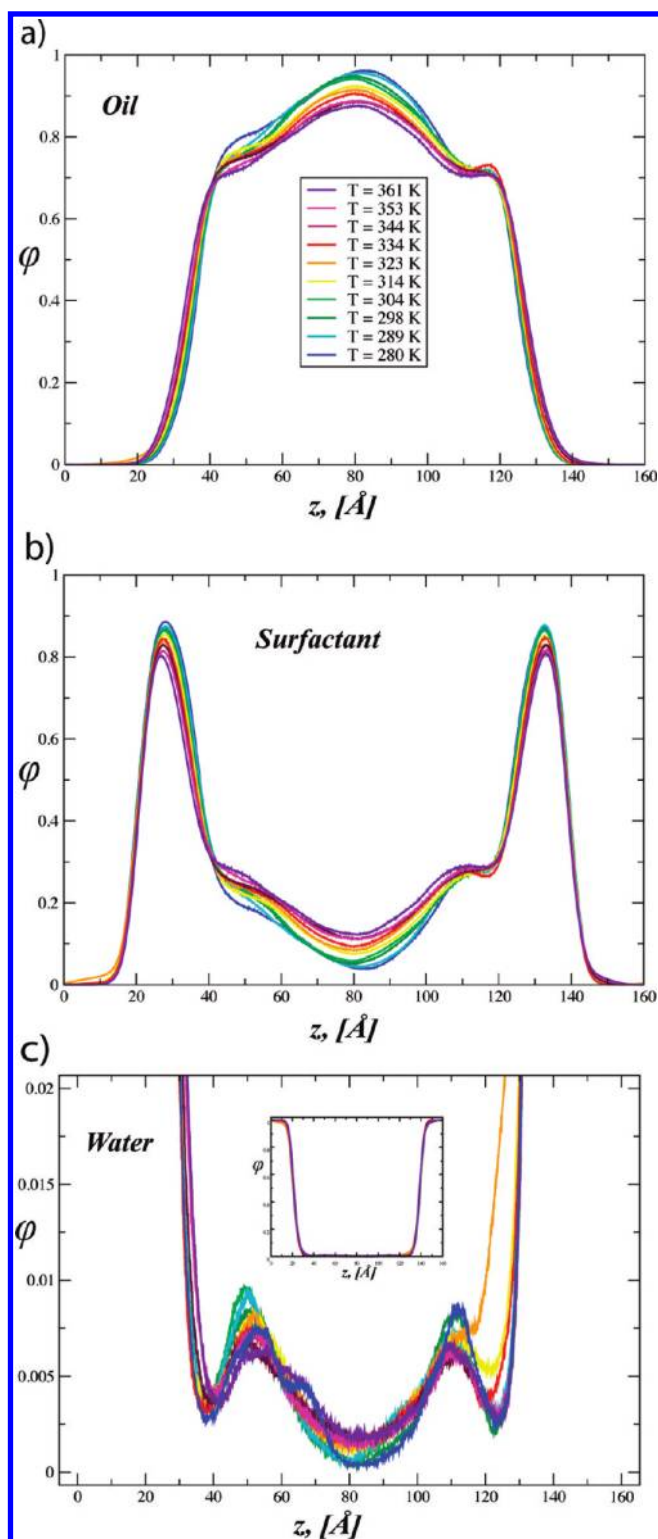
Figure 5. NFDs for (a) oil, (b) surfactant, and (c) water for 10 temperatures chosen from 42 available. The subplot in (c) shows a full profile of the water NFD, whereas the main plot (c) shows the water profile only at low concentrations because water presence in the oil layer is still quite low compared to that in the rest of the system. The abscissa is a coordinate along the layers normal, which corresponds to a horizontal axis in Figure 1a. The ordinate is a number fraction calculated from eq 1.

molecules wrapped by surfactants were transported through oil to a water pocket at the opposite side. To investigate the

character of water penetration into the oil—surfactant interface, the number fraction distributions (NFDs) along the layer normal (z-axis) were calculated for all components

$$\phi^j(z) = \frac{N^j(z)}{N^{wat}(z) + N^{surf}(z) + N^{oil}(z)}$$

$$j = (\text{water, surfactant, oil}) \qquad (1)$$

Oil, water, and surfactant NFDs are plotted for several temperatures in Figure 5. It is seen that for all temperatures, there is a local increase in the water number fraction at positions $z = 50$ and 110, as well as an appearance of a "plateau" in the surfactant concentration gradient in the range of $z \in (40-60)$ and $(110-130)$ Å (see Figure 5a,b). The oil NFD has local minima at the same regions, where most large water—surfactant aggregates are situated (see Figure 1a,c).

With increasing temperature, the surfactant NFD spreads out, and surfactant layers become more friable to water and oil intrusions (see Figure 5b). The presence of the surfactant molecules in the oil layer significantly grows, as expected, because nonionic surfactants are known to become more oleophilic with temperature increase.[42] At the same time, as the temperature is elevated, the water concentration in oil increases, which is accompanied by the spreading of the water—surfactant complexes traveling through bulk oil (see Figure 5c). As for the oil distribution profile, it spreads out as well, and oil actively penetrates through the surfactant layers, creating more direct water—oil contacts (see Figure 5a).

CONCLUSIONS

MD simulations help to provide detailed microscopic information, which otherwise is quite difficult to extract from experimental or theoretical studies. In the current paper, we reported results obtained from extensive atomistic REMD simulations on a nonionic ternary mixture water/octane/C_9E_3. The total simulation time in this work was near 1 μs, which represents by far the largest atomistic simulation of a microemulsion system to date.

We observed the nonequilibrium relaxation dynamics of the ternary system in a wide range of temperatures (7—88 °C) and studied the formation and transport of the water—surfactant complexes. We showed that surfactants play the role of an effective solvent for water molecules, facilitating water transport through the oil slab. We also found that a polar solvation cage created by surfactant molecules is highly dynamic; therefore, there is no specificity in hydrogen bond formation with respect to any particular surfactant oxygens. However, the majority of water oxygens form a hydrogen bond with the terminal hydrogen of a surfactant head (see Figure 4).

One of the fascinating observations in this work is that the major amount of water solubilized by the surfactant is situated in pockets on or at the border between surfactant and oil layers and is not homogeneously distributed in the surfactant—oil slab (see Figure 5). We also detected that with increasing temperature, the larger aggregates detach from the interface and travel through the oil layer, raising the overall water presence in oil.

Despite the fact that water—surfactant complexes vary in topology and sizes, our cluster analysis showed that the majority of these complexes do not form dense water cores, thus providing evidence for the hydrated surfactants transport mechanism[12,16,17] (see Figure 2).

It will be interesting to investigate the transport mechanisms of other species in the future work, such as weak acids or small

6507

dx.doi.org/10.1021/jp201431u |*J. Phys. Chem. B* 2011, 115, 6503–6508

ions, as well as their effects on water permeation. Also, calculation of such important characteristics as the diffusion, partition, and permeability coefficients and their dependences on temperature would be of great fundamental as well as applied biological and industrial interest.

■ AUTHOR INFORMATION

Corresponding Author
*E-mail: gpapoian@umd.edu.

■ ACKNOWLEDGMENT

■ REFERENCES

(1) Kumar, P.; Mittal, K. *Handbook of Microemulsion Science and Technology*; Marcel Dekker: New York, 1999.

(2) McCain, D. C.; Markley, J. L. *FEBS Lett.* **1985**, *183*, 353–358.

(3) Simons, R. *J. Membr. Sci.* **1993**, *82*, 65–73.

(4) Bart, H. J.; Jungling, H.; Ramaseder, N.; Marr, R. *J. Membr. Sci.* **1995**, *102*, 103–112.

(5) Marrink, S. J.; Berendsen, H. J. C. *J. Phys. Chem.* **1996**, *100* (41), 16729–16738.

(6) Courel, M.; Dornier, M.; Rios, G. M.; Reynes, M. *J. Membr. Sci.* **2000**, *173*, 107–122.

(7) Krylov, A. V.; Pohl, P.; Zeidel, M. L.; Hill, W. G. *J. Gen. Physiol.* **2001**, *118*, 333–340.

(8) Fornasiero, F.; Tang, D.; Boushehri, A.; Prausnitz, J.; Radke, C. *J. Membr. Sci.* **2008**, *320*, 423–430.

(9) Grime, J. M. A.; Edwards, M. A.; Rudd, N. C.; Unwin, P. R. *Proc. Natl. Acad. Sci. U.S.A.* **2008**, *105*, 14277–14282.

(10) Mathai, J. C.; Tristram-Nagle, S.; Nagle, J. F.; Zeidel, M. L. *J. Gen. Physiol.* **2008**, *131*, 69–76.

(11) Lee, D.; Ashcraft, J. N.; Verploegen, E.; Pashkovski, E.; Weitz, D. A. *Langmuir* **2009**, *25*, 5762–5766.

(12) Colinart, P.; Delepine, S.; Trouve, G.; Renon, H. *J. Membr. Sci.* **1984**, *20*, 167–187.

(13) Clausse, D.; Pezron, I.; Gauthier, A. *Fluid Phase Equilib.* **1995**, *110*, 137–150.

(14) Zielinski, R. G.; Kline, S. R.; Kaler, E. W.; Rosov, N. *Langmuir* **1997**, *13*, 3934–3937.

(15) Topgaard, D.; Malmborg, C.; Soderman, O. *J. Magn. Reson.* **2002**, *156*, 195–201.

(16) Wen, L.; Papadopoulos, K. D. *J. Colloid Interface Sci.* **2001**, *235*, 398–404.

(17) Wen, L.; Papadopoulos, K. D. *Colloids Surf., A* **2000**, *174*, 159–167.

(18) Evilevitch, A.; Jonsson, B. T.; Olsson, U.; Wennerstrom, H. *Langmuir* **2001**, *17*, 6893–6904.

(19) Deen, G. R.; Oliveira, C. L. P.; Pedersen, J. S. *J. Phys. Chem. B* **2009**, *113*, 7138–7146.

(20) Deen, G. R.; Pedersen, J. S. *J. Phys. Chem. B* **2010**, *114*, 7769–7776.

(21) Fisher, L. R.; Parker, N. S. *Biophys. J.* **1984**, *46*, 253–258.

(22) Evilevitch, A.; Rescic, J.; Jonsson, B.; Olsson, U. *J. Phys. Chem. B* **2002**, *106*, 11746–11757.

(23) Jeon, J.; Voth, G. A. *Biophys. J.* **2008**, *94*, 3497–3511.

(24) Orsi, M.; Sanderson, W. E.; Essex, J. W. *J. Phys. Chem. B* **2009**, *113*, 12019–12029.

(25) Wang, Y.; Cohen, J.; Boron, W. F.; Schulten, K.; Tajkhorshid, E. *J. Struct. Biol.* **2007**, *157*, 534–544.

(26) Aksimentiev, A.; Schulten, K. *Biophys. J.* **2005**, *88*, 3745–3761.

(27) Shinoda, W.; Mikami, M.; Baba, T.; Hato, M. *J. Phys. Chem. B* **2004**, *108*, 9346–9356.

(28) Luo, Y.; Roux, B. *J. Phys. Chem. Lett.* **2010**, *1*, 183–189.

(29) Bohanon, T. M.; Lee, A.; Ketterson, J. B.; Dutta, P. *Langmuir* **1992**, *8*, 2497–2500.

(30) Danov, K. D.; Kralchevsky, P. A.; Stoyanov, S. D. *Langmuir* **2010**, *26*, 143–155.

(31) Pocivavsek, L.; Dellsy, R.; Kern, A.; Johnson, S.; Lin, B.; Lee, K. Y. C.; Cerda, E. *Science* **2008**, *320*, 912–916.

(32) Case, D. A.; Cheatham, T. E.; Darden, T.; Gohlke, H.; Luo, R.; Merz, K. M.; Onufriev, A.; Simmerling, C.; Wang, B.; Woods, R. *J. Comput. Chem.* **2005**, *26*, 1668–1688.

(33) Wang, J.; Wolf, R. M.; Caldwell, J. W.; Kollman, P. A.; Case, D. A. *J. Comput. Chem.* **2004**, *25*, 1157–1174.

(34) Wang, J.; Wang, W.; Kollman, P. A.; Case, D. A. *J. Mol. Graphics Modell.* **2006**, *25*, 247260.

(35) Miyamoto, P. A., S.; Kollman *J. Comput. Chem.* **1992**, *13*, 952–962.

(36) Kohlbacher, O.; Lenhof, H. P. *Bioinformatics* **2000**, *16*, 815–824.

(37) Abel, S.; Waks, M.; Marchi, M.; Urbach, W. *Langmuir* **2006**, *22*, 9112–9120.

(38) Senapati, S.; Berkowitz, M. L. *J. Phys. Chem. B* **2003**, *107*, 12906–12916.

(39) Chen, Y.-J.; Xu, G.-Y.; Yuan, S.-L.; Sun, H.-Y. *Colloids Surf., A* **2006**, *273*, 174–178.

(40) Nymeyer, H. *J. Chem. Theory Comput.* **2008**, *4*, 626–636.

(41) Abraham, M. J.; Gready, J. E. *J. Chem. Theory Comput.* **2008**, *4*, 1119–1128.

(42) Winsor, P. A. *Trans. Faraday Soc.* **1948**, *44*, 376–398.